Supporting Information for "Active Radiative Thermal Switching with Graphene Plasmon Resonators"

Ognjen Ilic,[1] Nathan H. Thomas,[2] Thomas Christensen,[3] Michelle C. Sherrott,[1]
Marin Soljačić,[3] Austin J. Minnich,[2] Owen D. Miller,[4] and Harry A. Atwater[1]

[1]*Department of Applied Physics and Materials Science, California Institute of Technology, Pasadena, CA 91125, USA*
[2]*Department of Engineering and Applied Science, California Institute of Technology, Pasadena, CA 91125, USA*
[3]*Department of Physics, Massachusetts Institute of Technology, Cambridge, MA 02139, USA*
[4]*Department of Applied Physics and Energy Sciences Institute, Yale University, New Haven, CT 06511, USA*

I. BEYOND THE LOCAL RESPONSE APPROXIMATION (LRA) CONDUCTIVITY

The broadband spectrum of thermal radiation implies that achieving an OFF state of the proposed thermal switch necessitates strong spectral separation between plasmonic resonances of the emitter and the absorber side. Consequently, the two graphene structures must have significantly different carrier concentrations. For example, for low mobilities in the sheet-sheet case (Fig. 2), the OFF states are realized for Fermi levels at the respective ends of the allowed range, namely $E^{\rm off}_{1(2)} = E_{\rm min(max)}$. Because $E_{\rm max} \gg E_{\rm min}$, the dispersion of the resulting mode will lie well inside the region of Landau damping for the lower-doped graphene sheet. To fully assess the contribution of these high-momentum plasmons (that is, high-momentum relative to the Fermi momentum of the lower-doped graphene), we adopt the full nonlocal conductivity (i.e. incorporate momentum-dispersion in addition to frequency-dispersion); moreover, we include the temperature-dependence of the nonlocal conductivity by exploiting an integral identity due to Maldague [1, 2]. In Fig. S1, we compare the dispersion relation and the spectral dependence of $\Phi(\omega)$, for LRA and RPA conductivities. We find negligible difference in the integrated heat transfer (e.g. for mobility $\mu = 10^3$ cm^2/Vs we obtain $< 1\%$ difference between the RPA and the LRA results), for $d = 100$ nm separation. This observation is in accordance with similar considerations of nonlocal effects in the context of graphene RHT [3], and demonstrates the validity of a local-response treatment.

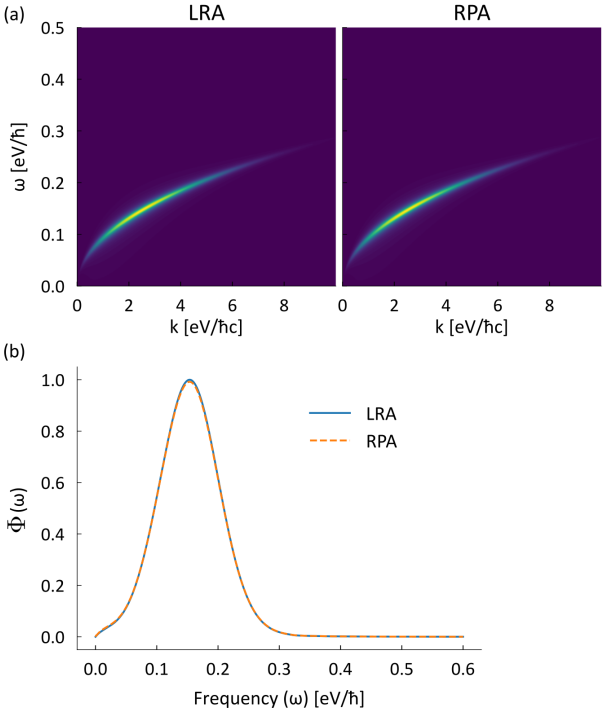

FIG. S1. Comparison of the LRA and the RPA graphene conductivity models. (a) Effective dispersion for the OFF state for the 2-sheet configuration of Fig. 2 for the case of mobility μ =10^3cm^2/Vs and $E^{\rm off}_{1(2)} = E_{\rm min(max)}$. (b) The corresponding spectral transfer function $\Phi(\omega)$.

II. EXPRESSIONS FOR THE RHT INVOLVING DIPOLAR STRUCTURES

In the dipolar limit, the radiative heat transfer between a resonator and its environment can be calculated using the relevant Green's functions [4, 5]:

$$H = \int_0^\infty {\rm d}\omega \left[\Theta(\omega, T_1) - \Theta(\omega, T_2)\right] \times \\ \times \frac{2\omega^2 \mu_0 \epsilon_0}{\pi} \sum_{i=x,y,z} {\rm Im}[\alpha_i(\omega)] {\rm Im}\left[\overleftrightarrow{\mathbf{G}}(\omega, \mathbf{r}_0)\right]_{ii} \tag{1}$$

where $\boldsymbol{\alpha}$ is the polarizability of the resonator (given by Eq. (3)of the main text), and $\overleftrightarrow{\mathbf{G}}$ is the Green tensor at the resonator position $\mathbf{r}_0$. For the case of two dipolar resonators in the near-field, we have:

$$\left[\overleftrightarrow{\mathbf{G}}(\omega)\right]_{ii} = \frac{1}{16\pi^2 k^2 R^6} \left[\alpha_i - \alpha_i \frac{6R_i^2}{R^2} + \frac{9R_i^2}{R^4} \sum_j \alpha_j R_j^2\right] \tag{2}$$

where R is the distance between the dipoles, and $k = \omega/c$. For two parallel disks with polarizabilities $\boldsymbol{\alpha}_{1,2} = \alpha(1,1,0)^T$, separated along the z axis a distance d apart, we have

$$\left[\overleftrightarrow{\mathbf{G}}(\omega)\right]_{xx} = \frac{1}{16\pi^2 k^2 d^6}\alpha(\omega) \\ \left[\overleftrightarrow{\mathbf{G}}(\omega)\right]_{yy} = \frac{1}{16\pi^2 k^2 d^6}\alpha(\omega) \\ \left[\overleftrightarrow{\mathbf{G}}(\omega)\right]_{zz} = 0 \tag{3}$$

Substituting Eq. (3) into Eq. (1), we recover the expression for the spectral heat transfer function, namely

$$\Phi(\omega, d) = \frac{2}{8\pi^3}\frac{1}{d^6}{\rm Im}(\alpha_1){\rm Im}(\alpha_2) \tag{4}$$

In a similar manner, for the case when the second object is an extended planar interface, the Green tensor is given by:

$$\overleftrightarrow{\mathbf{G}} = \frac{ik}{8\pi}\int_0^\infty \frac{s}{s_z} \begin{bmatrix} r_s - s_z^2 r_p & 0 & 0 \\ 0 & r_s - s_z^2 r_p & 0 \\ 0 & 0 & 2s^2 r_p \end{bmatrix} e^{2i\kappa d} {\rm d}s \tag{5}$$

where $s \equiv q/k$, $s_z \equiv \kappa/k$; k,q,κ are the total, parallel, and the perpendicular wave-vectors, respectively; r_p and r_s are the Fresnel reflection coefficients for the planar interface, for the p (TM) and s (TE) polarization, re-

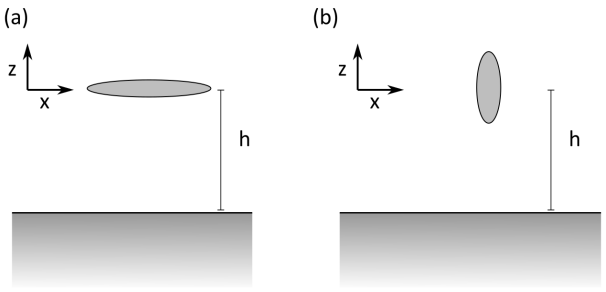

FIG. S2. Schematic for the NF-RHT calculation between a planar structure and a disk in a parallel (a) and a perpendicular (b) orientation.

spectively; and h is the height above the planar interface (see Fig. S2).

For a disk in a parallel configuration (Fig. S2a), we write its polarizability as $\boldsymbol{\alpha} = \alpha(1,1,0)^T$, and the spectral transfer function Φ becomes

$$\Phi_{\parallel}(\omega,h) = \frac{\omega^3}{4\pi^2c^3} 2\mathrm{Im}(\alpha)\mathrm{Re}\left[\int_0^\infty \frac{s}{s_z}\left(r_s - s_z^2 r_p\right) e^{2i\kappa h}\mathrm{d}s\right] \tag{6}$$

where the factor of 2 accounts for the two identical polarizations x, y. For a disk in a perpendicular configuration (Fig. S2b), the polarizability is $\boldsymbol{\alpha} = \alpha(0,1,1)^T$. Similarly, the transfer function simplifies to

$$\begin{aligned}\Phi_{\perp}(\omega,h) =& \frac{\omega^3}{4\pi^2c^3}\mathrm{Im}(\alpha)\times \\ &\times\left(\mathrm{Re}\left[\int_0^\infty \frac{s}{s_z}\left(r_s - s_z^2 r_p\right) e^{2i\kappa h}\mathrm{d}s\right] + \right. \\ &\left. + \mathrm{Re}\left[\int_0^\infty \frac{s}{s_z} 2s^2 r_p e^{2i\kappa h}\mathrm{d}s\right]\right)\end{aligned} \tag{7}$$

In the nonretarded limit ($q \gg k$), we note $\kappa \approx iq$, $s_z \approx iq$, which allows us to further approximate the integrals above

$$\begin{aligned}\mathrm{Re}\left[\int_0^\infty \frac{s}{s_z}\left(r_s - s_z^2 r_p\right) e^{2i\kappa h}\mathrm{d}s\right] &\approx \int_0^\infty (\mathrm{Im}(r_s) + \\ &+ \frac{q^2}{k^2}\mathrm{Im}(r_p))e^{-2qh}\frac{\mathrm{d}q}{k} \\ \mathrm{Re}\left[\int_0^\infty \frac{s}{s_z} 2s^2 r_p e^{2i\kappa h}\mathrm{d}s\right] &\approx \int_0^\infty 2\frac{q^2}{k^2}\mathrm{Im}(r_p)e^{-2qh}\frac{\mathrm{d}q}{k}\end{aligned} \tag{8}$$

As the optical response in the near field is dominated by surface plasmons, we focus on r_p, the p-polarized reflection coefficient. In this limit, we can relate the parallel (6) and the perpendicular (7) transfer function:

$$\begin{aligned}\Phi_{\perp}(\omega,h) &\approx \frac{3}{2}\Phi_{\parallel}(\omega,h) \\ &\approx \frac{3}{4\pi^2}\mathrm{Im}(\alpha)\int_0^\infty q^2\mathrm{Im}(r_p)e^{-2qh}\mathrm{d}q\end{aligned} \tag{9}$$

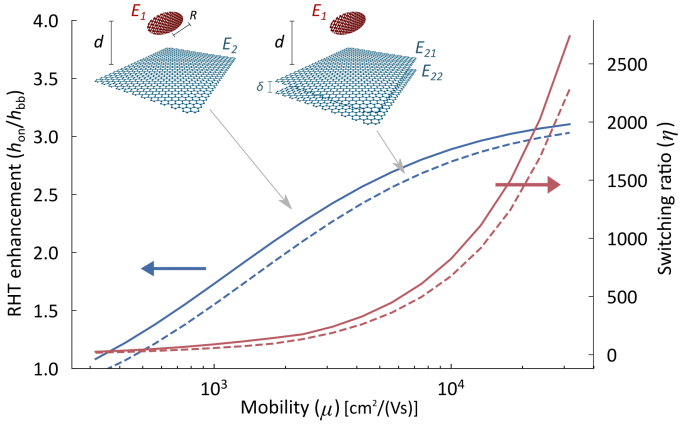

FIG. S3. (a) Thermal switching between a disk and a graphene stack, in a parallel configuration. RHT enhancement $h_{\mathrm{on}}/h_{\mathrm{bb}}$ (left) and the switching ratio $\eta = h_{\mathrm{on}}/h_{\mathrm{off}}$ (right) for a disk-sheet (solid) and a disk-stack (dashed) configuration. The disk is parallel to the sheet/stack. Here, T =300K, R =25nm, d =100nm, δ =10nm. Note that the radiative thermal conductance $h_{\mathrm{on(off)}}$ is normalized to the disk area ($A = \pi R^2$).

III. POLARIZABILITY MODEL FOR A GRAPHENE RESONATOR; FIRST-ORDER APPROXIMATION TO RTC

Resonator	ζ_1	Δ_1	Δ_1^2/ζ_1^3
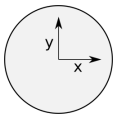	1.940	0.924	0.117
	1.686	0.859	0.154
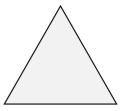	1.200	0.683	0.270
	(x) 1.118 (y) 2.981	0.939 0.842	0.631 0.027

TABLE S1. Dimensionless eigenfrequencies (ζ_1) and normalization factors (Δ_1) associated with Eq. (3) of the main text. All resonators have the same area A, and only the lowest energy (and the strongest) mode is considered. Characteristic length scale is defined as $L \equiv \sqrt{A}$. For the ellipse, the aspect ratio is 2:1.

For two resonators of the same shape, size, and Fermi level (such as in an ON state), we can simplify the ex-

pression for the radiative thermal conductance:

$$h(T) = \frac{1}{A}\int_0^\infty d\omega \sum_{j\in\hat{r}} \frac{\partial\Theta}{\partial T}(\omega)\frac{\lambda_j}{8\pi^3 d^6}\left[\mathrm{Im}(\alpha)\right]^2 \tag{10}$$

where

$$\frac{\partial\Theta}{\partial T}(\omega) = k_B\left(\frac{\hbar\omega}{k_BT}\right)^2 \frac{e^{\hbar\omega/k_BT}}{\left(e^{\hbar\omega/k_BT}-1\right)^2} \tag{11}$$

$$\mathrm{Im}(\alpha) = 2L^3\sum_\nu \Delta_\nu \mathrm{Im}\left(\frac{1}{\zeta_\nu - \zeta(\omega)}\right) \tag{12}$$

where $\zeta(\omega) = 2i\epsilon_0\omega L/\sigma(\omega)$. We can further simplify (12) as:

$$\mathrm{Im}(\alpha) = 2L^3\sum_\nu \Delta_\nu \frac{\zeta_I}{\left(\zeta_\nu-\zeta_R\right)^2+\zeta_I^2} \tag{13}$$

where $\zeta \equiv \zeta_R + i\zeta_I$ (with implicit dependence on frequency). Substituting back into (10), we get

$$h(T) = \frac{(2L^3)^2}{8\pi^3 A d^6}\sum_{j\in\hat{r}}\lambda_j \times \sum_\nu \int_0^\infty \mathrm{d}\omega \frac{\partial\Theta}{\partial T}(\Delta_\nu^j)^2 \frac{\zeta_I^2}{\left[\left(\zeta_\nu-\zeta_R\right)^2+\zeta_I^2\right]^2} \tag{14}$$

Assuming slowly variying $\frac{\partial\Theta}{\partial T}$ relative to the squared Lorentzian peaked at ω_j given by $\zeta_\nu^j = \zeta_R(\omega_\nu^j)$, we can further approximate

$$h(T) = \frac{(2L^3)^2}{8\pi^3 A d^6}\sum_{j\in\hat{r}}\lambda_j \sum_\nu (\Delta_\nu^j)^2 \frac{\partial\Theta(\omega_\nu^j)}{\partial T} I_\nu^j \tag{15}$$

where we define

$$I_\nu^j \equiv \int_0^\infty \mathrm{d}\omega \frac{\zeta_I^2}{\left[\left(\zeta_\nu-\zeta_R\right)^2+\zeta_I^2\right]^2} \tag{16}$$

To approximate (16), we assume the dominant contribution to graphene conductivity for a resonantly-coupled system comes from intraband transitions. Hence, we express the optical conductivity as $\sigma \simeq \sigma_{\mathrm{intra}} = ie^2E_F/(\pi\hbar^2(\omega+i\gamma))$. Defining $\beta \equiv \frac{2\pi\epsilon_0\hbar^2}{e^2}\frac{L}{E_F}$, we can further express $\zeta_R = \beta\omega^2$, $\zeta_I = \beta\omega\gamma$, and the resonant frequencies at $\omega_\nu^j \simeq \sqrt{\zeta_\nu^j/\beta}$. Correspondingly, in the intraband (Drude) approximation, I_ν^j is given by

$$I_\nu^j \simeq \left(\frac{e^2E_F}{2\pi\epsilon_0\hbar^2L}\right)^2 \int_0^\infty \mathrm{d}\omega \frac{(\omega\gamma)^2}{\left[\left(\omega_\nu^{j2}-\omega^2\right)^2+(\omega\gamma)^2\right]^2} = \frac{1}{\beta^2}\frac{\pi}{4\gamma}\frac{1}{\left(\omega_\nu^j\right)^2} = \frac{\pi}{4\gamma\beta\zeta_\nu^j} \tag{17}$$

Substituting back into (15), we have

$$h(T) = \frac{1}{A}\sum_{j\in\hat{r}}\sum_\nu \frac{\lambda_j}{2}\frac{\partial\Theta(\omega_\nu^j)}{\partial T}\frac{L^6}{d^6}\frac{1}{\gamma}\left(\frac{\Delta_\nu^j\omega_\nu^j}{2\pi\zeta_\nu^j}\right)^2 \tag{18}$$

where we (re)emphasize:

$$\omega_\nu^j \simeq \sqrt{\zeta_\nu^j/\beta}$$
$$\beta \equiv \frac{2\pi\epsilon_0\hbar^2}{e^2}\frac{L}{E_F}$$
$$\gamma = \frac{ev_F^2}{\mu E_F}$$

To find the optimal Fermi level that maximizes heat transfer for a given resonator size, temperature, and mobility, we take the derivative of Eq. (18) with respect to E_F. Expressing β and γ in terms of ω_ν^j and substituting back into (18), we observe the following dependence

$$h(T) \propto \sum_j\sum_\nu \frac{\partial\Theta(\omega_\nu^j)}{\partial T}\left(\omega_\nu^j\right)^4 \tag{19}$$

Further assuming that the heat transfer is dominated by a single mode (or a set of degenerate modes) at frequency ω_0, the desired functional dependence is equivalent (under substitution $x = \hbar\omega/k_BT$, and using (11)) to

$$f(x) = x^6\frac{e^x}{(e^x-1)^2} \tag{20}$$

which peaks at x_0 that satisfies

$$x_0\coth\left(\frac{x_0}{2}\right) = 6 \quad\rightarrow\quad x_0 \approx 5.9694 \tag{21}$$

Specifically, this implies that assuming complete control of the doping level, the optimal frequency of the peak spectral heat transfer between identical graphene resonators will (in this approximation) be given by $\hbar\omega_0 \approx 6k_BT$. Assuming the dominant response arises from mode(s) with oscillator strength Δ_1 and frequency ζ_1 (i.e. $\nu = 1$), we can further approximate the ON state radiative thermal conductance (and the corresponding Fermi levels $E_{1,2} = E_{\mathrm{ON}}$) as

$$h_{\mathrm{ON}} \approx 116.23\left(\frac{\epsilon_0k_B^5T^4}{2\pi\hbar^2e^3v_F^2}\right)\frac{1}{A}\frac{\lambda_S}{2}\mu\frac{L^7}{d^6}\frac{\Delta_1^2}{\zeta_1^3} \tag{22}$$

$$E_{\mathrm{ON}} \approx 71.27\left(\frac{\pi\epsilon_0k_B^2T^2}{e^2}\right)\frac{L}{\zeta_1} \tag{23}$$

where $\lambda_S \equiv \sum_{j\in\hat{r}}\lambda_j$ is the sum of all numerical prefactors for the mode(s) associated with Δ_1 and ζ_1. Figure S4 compares the approximated results from Eqs. (22) and (23) to the full numerical calculations for graphene disks. We observe that the approximated expressions become more accurate for larger disk resonators where the

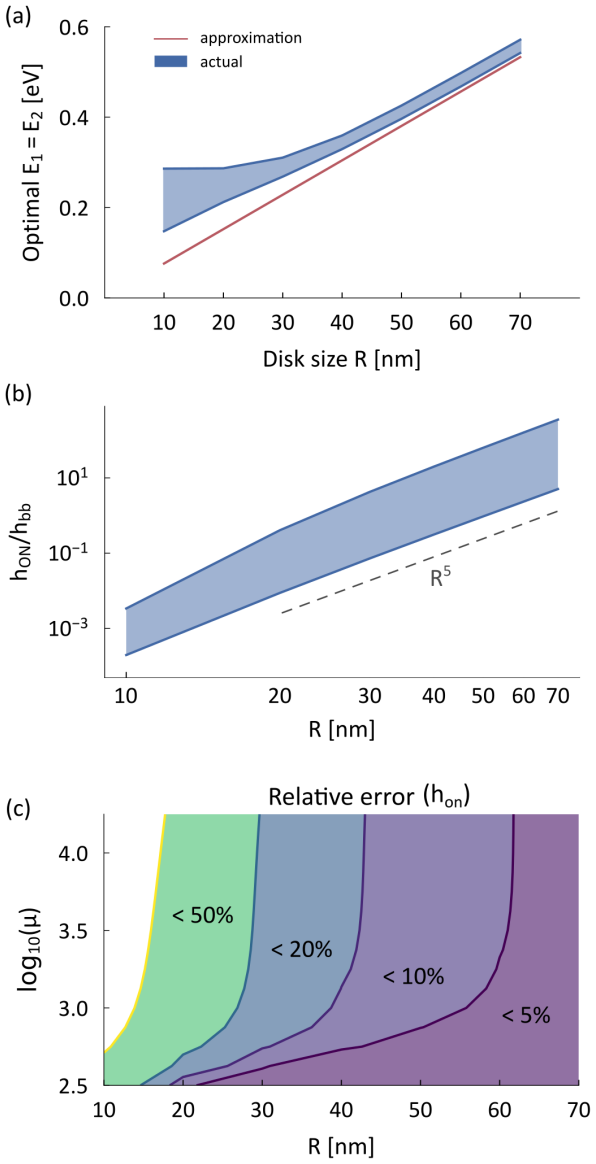

FIG. S4. (a) Optimal Fermi levels $E_1^{\rm on} = E_2^{\rm on}$, (b) size-dependence, and (c) the corresponding maximum radiative thermal conductance $h_{\rm ON}$ for graphene disks ($L \equiv \sqrt{\pi R^2}$): comparison between the actual (full numerical evaluation of Eq. (10)) and the approximated result from Eqs. (22) & (23). The shaded regions in (a) and (b) correspond to a range of mobility values (i.e. the y-axis in (c)). Note that the $\propto R^5$ dependence in (b) applies to the $h_{\rm on}/h_{\rm bb}$ enhancement, whereas $h_{\rm on} \propto R^7$, in accordance with Eq. (4) of the main text.

optimal Fermi levels are higher (and the assumption of intraband-dominated conductivity more valid).

Finally, these approximations allow us to directly compare different resonator shapes. Using the values from Table S1, we immediately see that two disks should have the weakest ON state thermal conductance compared to two squares, triangles, or (2:1) ellipses of the same area. Full numerical simulations for these shapes indeed confirm this conclusion.

IV. RADIATIVE THERMAL SWITCHING: SEPARATION DISTANCE, SUBSTRATE

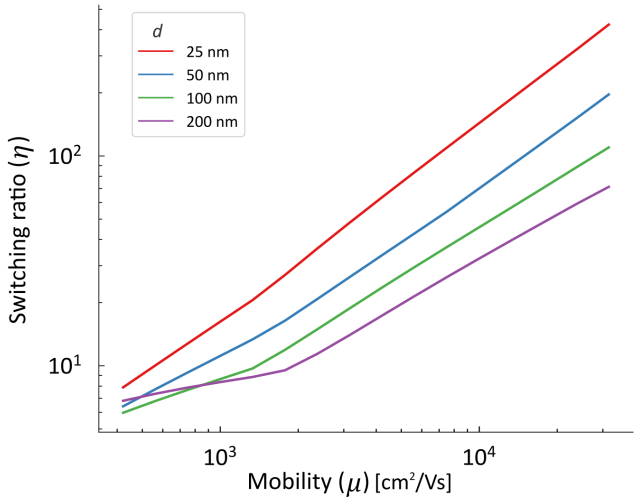

FIG. S5. Switching ratio for the sheet-sheet configuration as a function of mobility, for several separation distances d. We observe similar trends for the sheet-stack configuration.

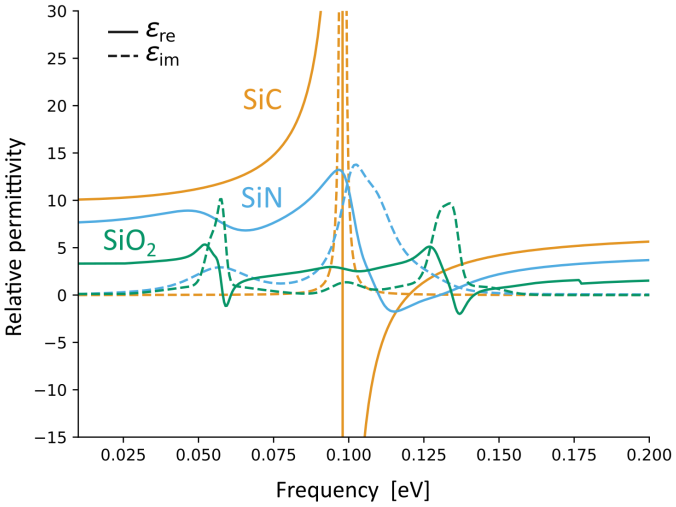

FIG. S6. Relative dielectric permittivity for SiC [6], SiN [7], and SiO_2 [8] in the relevant frequency range.

[1] Maldague, P. F. Many-body Corrections to the Polarizability of the Two-dimensional Electron Gas. *Surf. Sci.* **1978**, *73*, 296–302.

[2] Duppen, B. V.; Tomadin, A.; Grigorenko, A. N.; Polini, M. Current-induced Birefringent Absorption and Non-reciprocal Plasmons in Graphene. *2D Mater.* **2016**, *3*, 015011.

[3] Yu, R.; Manjavacas, A.; García de Abajo, F. J. Ultrafast Radiative Heat Transfer. *Nat. Commun.* **2017**, *8*.

[4] Mulet, J.-P.; Joulain, K.; Carminati, R.; Greffet, J.-J. Nanoscale Radiative Heat Transfer between a Small Particle and a Plane Surface. *Appl. Phys. Lett.* **2001**, *78*, 2931–2933.

[5] Novotny, L.; Hecht, B. *Principles of Nano-Optics*; Cambridge University Press, 2006.

[6] Spitzer, W. G.; Kleinman, D.; Walsh, D. Infrared Properties of Hexagonal Silicon Carbide. *Phys. Rev.* **1959**, *113*, 127–132.

[7] Cataldo, G.; Beall, J. A.; Cho, H.-M.; McAndrew, B.; Niemack, M. D.; Wollack, E. J. Infrared Dielectric Properties of Low-stress Silicon Nitride. *Opt. Lett.* **2012**, *37*, 4200.

[8] Kitamura, R.; Pilon, L.; Jonasz, M. Optical Constants of Silica Glass from Extreme Ultraviolet to Far Infrared at Near Room Temperature. *Appl. Opt.* **2007**, *46*, 8118.